Chemical Engineering Journal 105 (2005) 71–79

Chemical Engineering Journal

www.elsevier.com/locate/cej

Interfacial area in a reactor with helicoidal flow for the two-phase gas–liquid system

S. Wroński*, R. Hubacz, T. Ryszczuk

Faculty of Chemical and Process Engineering, Warsaw University of Technology, ul. Waryńskiego 1, 00-645 Warszawa, Poland

Received 1 July 2003; accepted 30 April 2004

Abstract

Interfacial area was measured in a helicoidal reactor for the two-phase gas–liquid flow. Measurements were accomplished using the method of oxygen chemical absorption in alkaline solutions of $Na_2S_2O_4$. The process parameters were varied within the following ranges: rotational speed of impeller from 0 to 2900 rpm; liquid mass flux from 2.7 to 100 kg/(m^2 s); volumetric flow ratio of gas and liquid from 0.125 to 1; ratio of impeller diameter to the outer reactor diameter from 0.54 to 0.92. Large values of the interfacial area were found. It was established that they depend mainly on the rotational speed of the rotor and to much less extent on the axial flow velocity. A correlation between changes in the interfacial area and changes in the flow structure within the reactor was also observed.

Keywords: Gas–liquid flow; Interfacial area; Helicoidal flow

1. Introduction

Helicoidal flow in an annular gap results from superposition of the axial and rotational flows caused by a rotational motion of an inner cylinder. This type of flow is commonly referred to in references as Couette–Taylor flow (CTF). For such a flow loss of stability is characteristic above a critical value of the rotational velocity of a rotor. Under an effect of inertial force, a secondary fluid motion appears in the form of cellular Taylor vortices. One of the first papers describing this phenomenon was published by Taylor [1]. The form of Taylor vortices in a single-phase helicoidal flow depends both on the rotor rotational frequency as well as on the axial flow [2,3]. The vortices assume a toroidal shape at the axial Reynolds number $Re < 40$, and a helicoidal one at $Re > 40$. Appearance of the Taylor vortices and combination of the axial flow with the rotational one result in that helicoidal the flow has the following features:

- low value of the axial dispersion with respect to the radial dispersion when compared to the other types of equipment [4]; owing to this property plug flow can be relatively well obtained in an apparatus with Couette–Taylor flow;
- possibility of independent control over mixing intensity and residence time in a reactor with such type of flow;
- Taylor vortices induce mild but effective mixing; this is favourable, e.g. in bioreactors [5,6].

The mentioned features result in increasing interest in applying Couette–Taylor flow in different processes. Recently published papers offer suggestions for application of helicoidal flow in the following processes:

- Photocatalytic reactions [7]
- Polymerisation reactions [8]
- Reversed osmosis [9]
- Precipitation [10]
- Blood detoxication [11]

Among the mentioned applications of helicoidal flow there are also those for multiphase systems. In the case of two-phase (gas–liquid) flow one can expect additional benefit from applying helicoidal flow, namely more intensive mass transfer between two phases and good conditions for dispersing gas phase at a low (unfavourable) ratio of gas and liquid phases.

Wroński et al. [12] and Dłuska et al. [13,14] studied this type of reactor and obtained high values of the volumetric mass transfer coefficients. Hubacz [15] determined power demand in a CTF reactor, and Hubacz and Wroński [16] suggested a regime map for a two-phase flow in a horizontal CTF reactor. A method that served in determination of dissipated power and applied in this work was described elsewhere [15].

* Corresponding author. Tel.:+48 22 660 6295; fax: +48 22 825 1440.
E-mail address: wronski@ichip.pw.edu.pl (S. Wroński).

1385-8947/$ – see front matter © 2004 Elsevier B.V. All rights reserved.
doi:10.1016/j.cej.2004.04.002

The aim of the present work is presentation of the results of determination of the gas–liquid interfacial area in helicoidal reactor as a function of hydrodynamic conditions. A chemical method based on absorption of oxygen in alkaline solutions of sodium dithionite was applied. From literature data on this method [22–24], it follows that within a wide range of sodium dithionite concentration reaction kinetics does not change significantly. Such a feature is of importance when interfacial area is determined in continuous flow reactors with widely changing reagent concentrations.

2. Experimental methods and equipment

Determinations of interfacial area were carried out in a helicoidal reactor. The main dimensions of the reactor are as follows: outer cylinder diameter $D_o = 37$ mm, length $L = 317$ mm, diameter of rotating cylinder $D_i = 20$; 26.5; and 34 mm. The outer and inner cylinders were made of plastic material.

The experimental apparatus is shown in Fig. 1. Helicoidal reactor (1) is its main part. The inner cylinder of the reactor is set into rotational movement by means of a driving gear consisting of a three-phase electrical motor (2) and a control device (3) enabling continuous regulation of the rotational speed of the impeller. Absorbed gas (O_2) is taken from a pressure cylinder (4) with absorbing solution from a tank (5). Electronic flow-meter (6) is applied to control and measure gas flow rate. Liquid flow rate is controlled using a peristaltic pump (7) and measured with rotameter (8). The temperatures at the inlet and the outlet of the reactor are determined using thermometers 9 and 10. Separator (12) serves to separate the reaction mixture leaving the reactor. Samples for analyses are withdrawn by means of three-way valves 13 and 14.

Before accomplishing interfacial area determination, a solution of desired NaOH concentration was prepared. The solution was then saturated with nitrogen and then a predetermined amount of sodium dithionite was added. The obtained mixture and gas were fed into the reactor. After stabilising process parameters (temperature, rotational speed of the rotor, liquid flow rate and the volumetric flow ratio of gas and liquid), liquid samples were withdrawn from the inlet and the outlet of the reactor to measure sodium dithionite concentration. The composition of the liquid phase was iodometrically analysed in presence of formaldehyde. The details of this method are given in [17]. Titration was carried out using a digital biurette and automatic pipette.

The initial concentration of NaOH was equal to 1 kmol/m^3. Concentration of sodium dithionite changed in the range of 0.01 to 0.2 kmol/m^3. Liquid mass flux varied between 2.7 and 100 kg/(m^2 s) while gas mass flux equalled 1.4–400 kg/(m^2 s), resulting in the volumetric flow ratio of gas and liquid from 0.125 to 1. Rotational speed of the rotor was changed from 0 to 2900 rpm. Owing to application of different rotor diameters (20–34 mm), the ratio of the impeller diameter to that of the outer diameter of the reactor could be obtained from 0.54 to 0.91. Temperature ranged from 20 to 30 °C.

The range of hydrodynamic parameters was assumed based on a predicted range of a real reactor performance, i.e. large residence time and relatively small gas holdup.

The chemical method based on absorption of oxygen in alkaline solutions of sodium dithionite was applied. This method of determination of interfacial area in gas–liquid contactors was suggested by Jhaveri and Sharma [18,19],

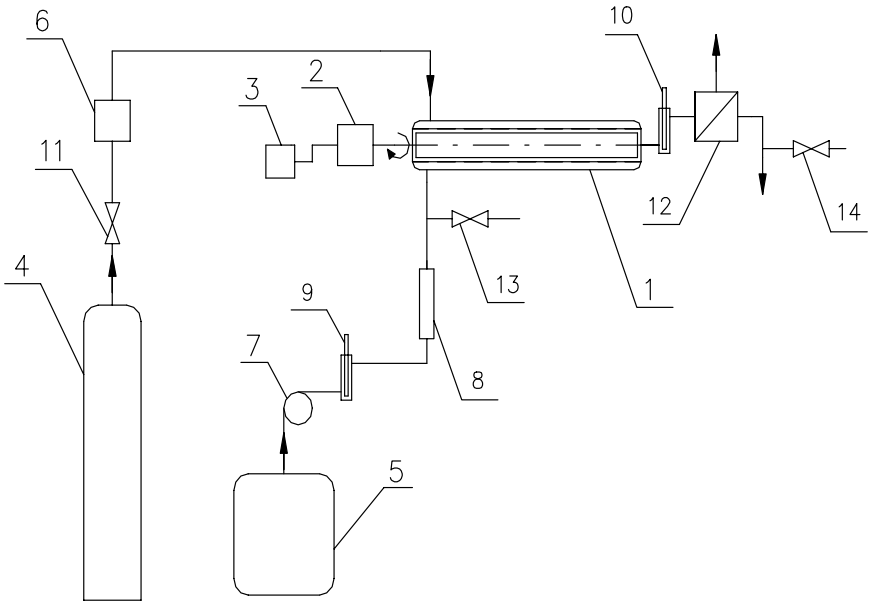

Fig. 1. Experimental equipment: (1) helicoidal reactor; (2) motor; (3) inverter; (4) oxygen cylinder; (5) vessel with alkaline solution of sodium dithionite; (6) gas flow rate control device; (7) peristaltic pump; (8) rotameter; (9, 10) termometers; (11) reducing valve; (12) separator; (13, 14) three-way valves.

Sahay and Sharma [20], Joshi and Sharma [21] and Camacho et al. [22–24].

Taking into account that oxidation of sodium dithionite with molecular oxygen described by the reaction:

$$S_2O_4^{2-} + O_2 + 2OH^- \rightarrow SO_3^{2-} + SO_4^{2-} + H_2O \quad (1)$$

undergoes within fast reaction regime and is of zero'th order with respect to oxygen concentration and 1.5-th order with respect to sodium dithionite concentration [22–24] and assuming that in the helicoidal reactor prevails plug flow, an expression enabling calculation of the interfacial area can be written according to the theory of absorption with simultaneous chemical reaction in the liquid phase [25,26] as follows:

$$a = \frac{4u_L([S_2O_4^{2-}]_{inlet}^{0.25} - [S_2O_4^{2-}]_{inlet}^{0.25})}{(2k)^{0.5}\sqrt{D_{O_2}[O_2]_i}L} \quad (2)$$

where [22]

$$k = 3.22 \times 10^5 \exp\left(-\frac{4250}{T}\right) \quad (3)$$

For this type of reaction, $[O_2]_0$, i.e. the oxygen concentration in the bulk of the liquid is equal zero.

The values of oxygen diffusivity in the liquid and oxygen concentration at the interface were substituted in Eq. (2) as the arithmetic averages from the values at the inlet and the outlet of the reactor. Because of small variations of the ionic strength of the solution during the course of the reaction under the conditions of practically constant pressure of O_2 and neglecting an effect of dissolved N_2 on oxygen solubility, oxygen concentration at the interface was determined based on the average value of the Henry's law coefficient.

The necessary physical and chemical properties were estimated as described in the article by Camacho et al. [22], except for the values of the Henry's law constant for the system oxygen–water, which were determined from an equation given by Moniuk et al. [27].

3. Results of experiments

Figs. 2 and 3 show selected results of the interfacial area measurements as a function of the rotational speed of impeller for the ratio of the inner and the outer cylinder diameter, η, equal to 0.54. All obtained experimental data on the interfacial area was published elsewhere [28,29].

Fig. 2 shows an effect of the mixing rate at different volumetric flow ratio of gas and liquid, β, at a constant liquid velocity, G, while Fig. 3 refers to an influence of different liquid velocities at a constant volumetric ratio of gas and liquid. The ratio, β, represents a nominal holdup value, calculated on the basis of the volumetric flow rates of both phases at the inlet to the reactor. Because of plug flow in both phases and the vortex structure, assumption of the lack of slip between the phases seems to be fully justified. It can

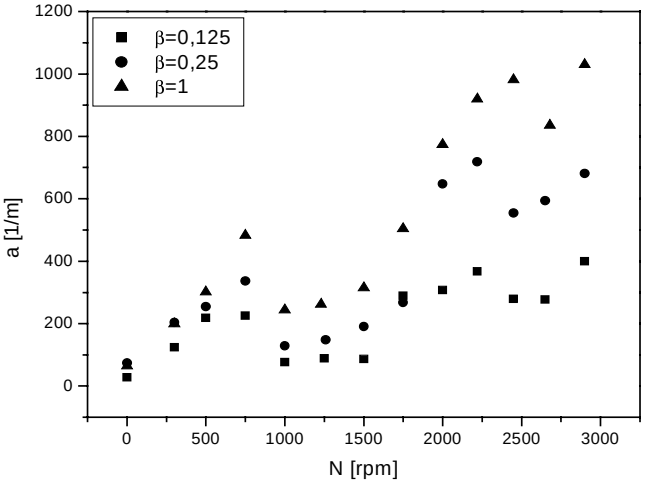

Fig. 2. Dependence of interfacial area on rotational speed of impeller at different values of β for $\eta = 0.54$ and $G = 11\,kg/(m^2\,s)$.

be seen that the interfacial area depends much on process parameters such as rotational speed of impeller and the volumetric ratio of gas and liquid, while liquid flow rate is of less importance. The former dependence does not have a monotonic character and in all experiments local extrema were detected. The whole range of the rotational speed of impeller can then be divided into three regions, for which an increase and decrease in the interfacial area with rotational speed of impeller were observed.

Diagrams $a = f(N)$ are similar for all hydrodynamic conditions. It seems then justified to assume that these changes are dependent on hydrodynamic regime of helicoidal flow (see below in Section 4).

The results of measurements of interfacial area are shown in Fig. 4 as a dependence on the parameter η at the constant values of other parameters such as liquid mass flux, G, and the volumetric gas and liquid flow ratio, β. It is evident that

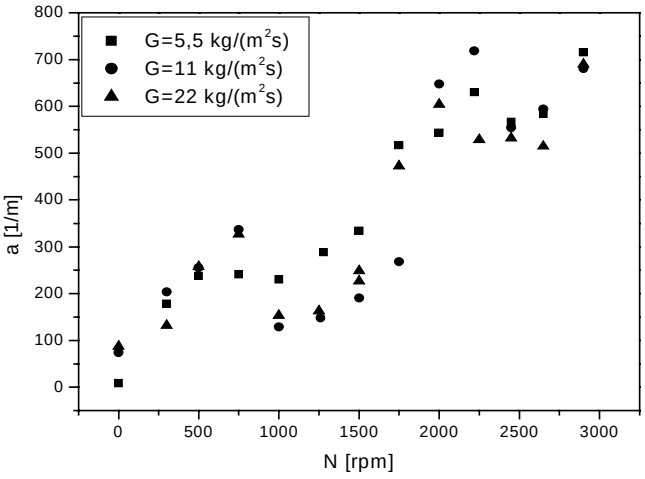

Fig. 3. Dependence of interfacial area on rotational speed of impeller at different values of G for $\eta = 0.54$ and $\beta = 0.25$.

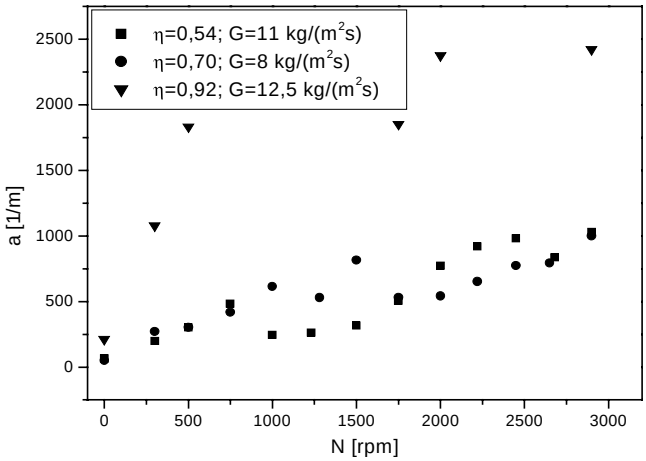

Fig. 4. Dependence of interfacial area on rotational speed of impeller at different values of η for $\beta = 1$.

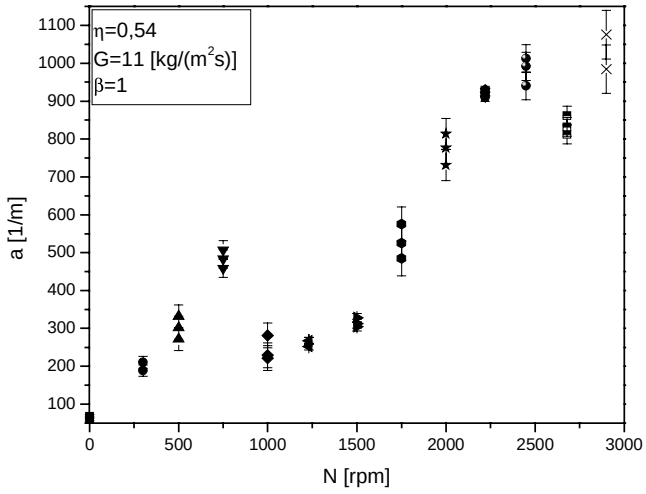

Fig. 5. Reproducibility of data.

the interfacial area strongly depends on the ratio between the inner and outer cylinder diameters, η.

Error bars for the results of one of the experimental series, shown earlier in Fig. 2, are demonstrated in Fig. 5. It is seen that replication of measurements at the same operational conditions do confirm that reproducibility of the applied method is satisfactory since the deviations from a mean values do not exceed 15%.

4. Discussion

Hubacz and Wroński [16] carried out investigations on the flow structure using a visualization method. Based on their own observations they suggested a map of the flow structures as a function of energy dissipated by the rotational motion. Contribution of the energy dissipated by the rotational motion is dominating in the overall dissipated energy in the system. The structure of helicoidal two-phase flow depends first of all on the rotational speed of the rotor and the gas

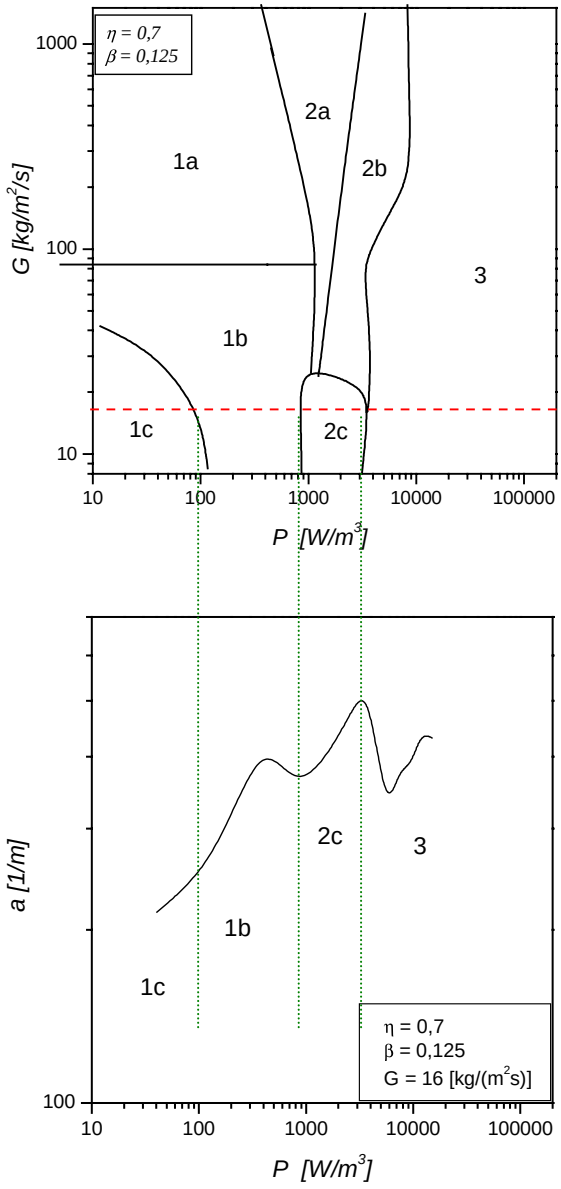

Fig. 6. Adjusting of the flow regions map with diagram of dependence $a = f(P)$ for $G = 16\,\mathrm{kg/(m^2\,s)}$.

holdup, while to much less extent on the liquid velocity and the gap width. The elaborated maps expressed in form of dissipated energy for the subsequent values of β and η are of general character [16].

Dependencies of the interfacial area on dissipated power coupled with the flow maps are shown in Figs. 6 and 7. The structure description of flow maps is given in Table 1 [16]. In the regions 1a, 1b, 1c, and 2a a stratified or slug flow are dominating while regions 2b and 2c are characterized by a transitional flow structure where two-phase cell vortices are present. In region 3 distinct, independent and—at the same time—parallel vortices are evident, with dominating liquid or gas phases. The results of interfacial area measurements indicate a clear dependence of changes in interfacial area separation on the flow structure in the reactor. A coupling

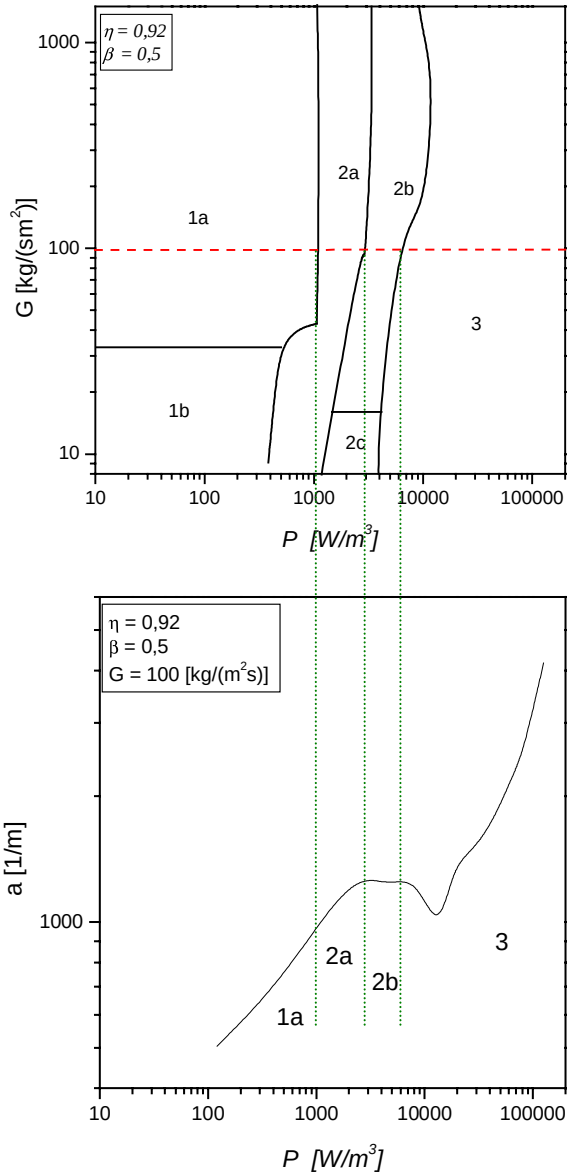

Fig. 7. Adjusting of the flow regions map with diagram of dependence $a = f(P)$ for $G = 100\,\mathrm{kg/(m^2\,s)}$.

between changes of interfacial area with the rotational speed of impeller with the map of flow structures seems to be evident. Since a dependence of interfacial area on the rotational speed of impeller is not a monotonic function, generalization of the obtained results is a complex problem, requiring extensive experimental and simulation studies. Comparisons (Figs. 6 and 7) were made for the same values of the volumetric flow ratios of gas and liquid, β, and the parameter η, indicating a current selected value of the liquid flow rate. In order to make such a comparison more clear, the experimental data are now displayed in form of smooth curves using a cubic B-spline connection (Figs. 6 and 7).

Table 1
Description of the flow structures

No.	Symbol	Name
1a	SL	Slug flow
1b	TR1	Transition flow
1c	ST	Stratified flow
2a	DSL	Disturbed slug flow
2b	TR2	Transition regime
2c	PE	Periodical flow
3	HR	High rotation flow

It is now possible to combine changes in the character of curves describing the dependence of interfacial area with the energy dissipated by the rotational motion. One can conclude that interfacial area, a, first increases due to intensification of mixing (regions 1, cf. Table 1) until a transition structure (regions 2) is attained. Then, as a result of the ordered flow structure (phase segregation), it decreases more or less. Further increase in the rotational speed of rotor leads to changes in the liquid and phase vortex structures (region 3), then finally the vortices collapse and a turbulent flow structure is formed, in consequence yielding significant enlargement of the interfacial area. At smaller values of η, a transition from the stratified or slug regions (1) into the transition regions (2) also results in a decrease of interfacial area.

A comparison of graphs $a = f(P)$ with the maps of the flow structures justifies an assumption that interfacial area depends on the flow structure. It is generally assumed that the best way in correlating the experimental data on the two-phase flows is to relate them to the values of dissipated energy per unit volume of the mixture (P). Since this parameter can be expressed as a function of the appropriate dimensionless numbers [15], as examples, the obtained results for a narrow and a wide gap were correlated in form of a function $a = f(Re_{rot})$, cf. Figs. 8 and 9. For a wide gap ($0.5 < \eta < 0.9$), a limiting value of $(Re_{rot})_1$ for transition from region 1 (cf. Table 1) to region 2 is equal to about 8000, while analogous transition from region 2 to 3 $(Re_{rot})_2$ corresponds to ca. 27,500. For a narrow gap ($\eta > 0.9$), the corre-

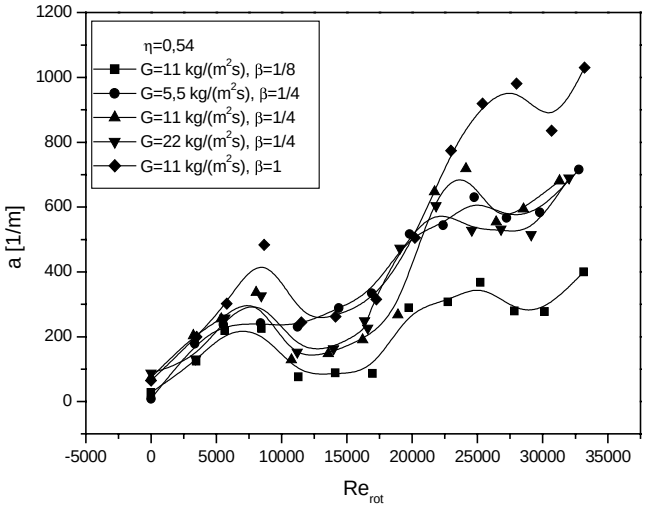

Fig. 8. Dependence of interfacial area on rotational Reynolds number for $\eta = 0.54$.

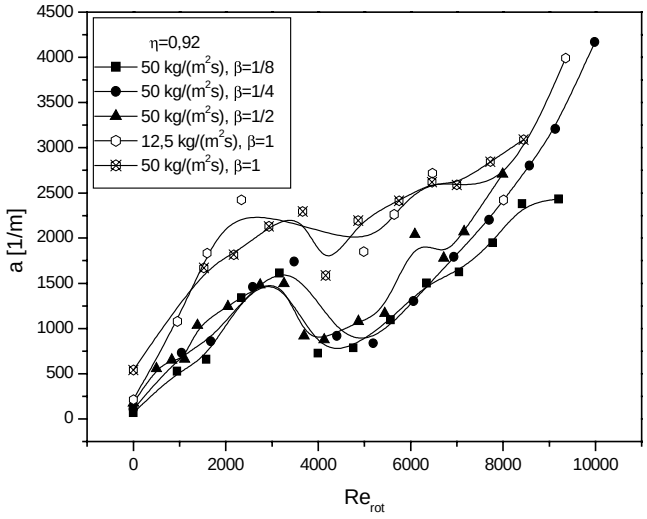

Fig. 9. Dependence of interfacial area on rotational Reynolds number for $\eta = 0.92$.

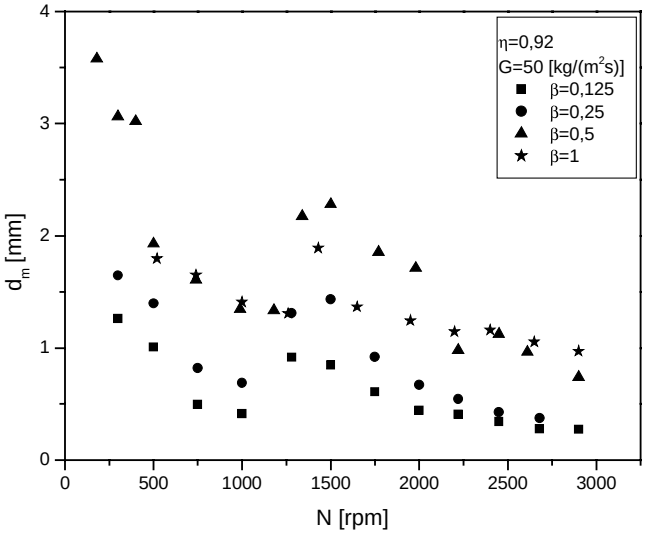

Fig. 11. Dependence of mean bubble size on rotational speed of impeller at different values of β and for $\eta = 0.92$ and $G = 50\,\mathrm{kg/(m^2\,s)}$.

sponding value of $(Re_{rot})_1$ amounts ca. 3500 while a limiting value of $(Re_{rot})_2$ has not been observed. Dependences of $a = f(Re_{rot})$ are located in a reasonable way, i.e. they indicate a dependence on β, such that at higher values of β we get higher values of the interfacial area. Previously mentioned small effect of the flow rate, G, is evident.

A dependence of the mean bubble diameter (based on the known interfacial area: $(d_m = 6\beta/(\beta+1)a)$ on the rotational velocity of the impeller for different gaps is shown in Fig. 10. It can be noticed that the gap width significantly affects the bubble size.

Effects of gas holdup on the bubble size are presented in Fig. 11. As expected, the mean bubble diameter increases with decreasing gas holdup. The same relationship has been observed for other gaps.

The mean bubble size obtained experimentally and estimated by photographic records, for the chosen conditions ($\eta = 0.92$, $\beta = 1/8$, $N = 1050\,\mathrm{rpm}$) was compared. Based on the photographic records the estimated bubble size is ca. 1 mm and this in principle corresponds to the results obtained from the chemical method of determination.

In order to verify the obtained results, interfacial area was determined using a method of chemical absorption of carbon dioxide in aqueous solutions of diethanoloamine (DEA) described in [30]. In contrast to the method in the system O_2–$Na_2S_2O_4$ determination of interfacial area is based on the concentration measurements in the gas phase. The results of these measurements carried out using two different methods at the same experimental conditions are shown in Fig. 12. The curves describing a dependence of interfa-

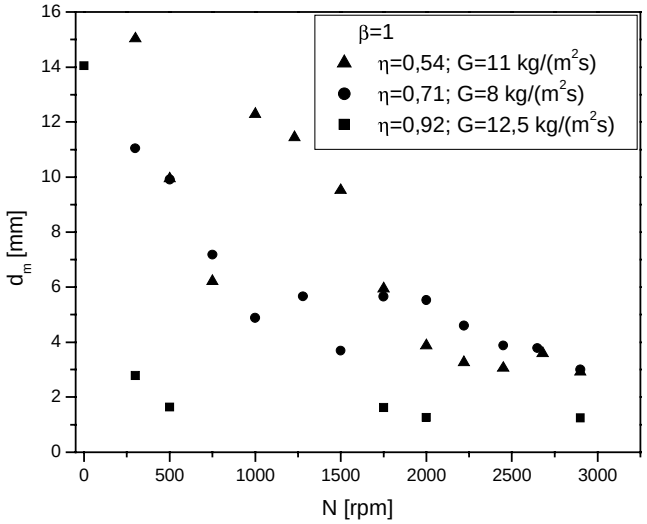

Fig. 10. Dependence of mean bubble size on rotational speed of impeller at different values of η and for $\beta = 1$.

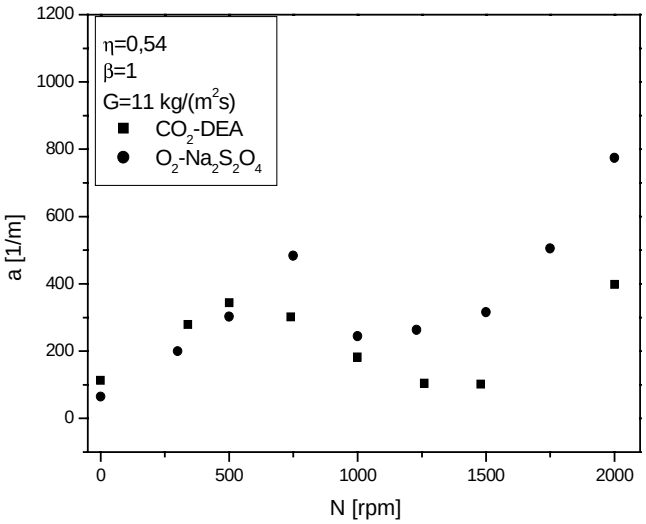

Fig. 12. Dependence of interfacial area on the rotational speed of impeller for two measurements methods.

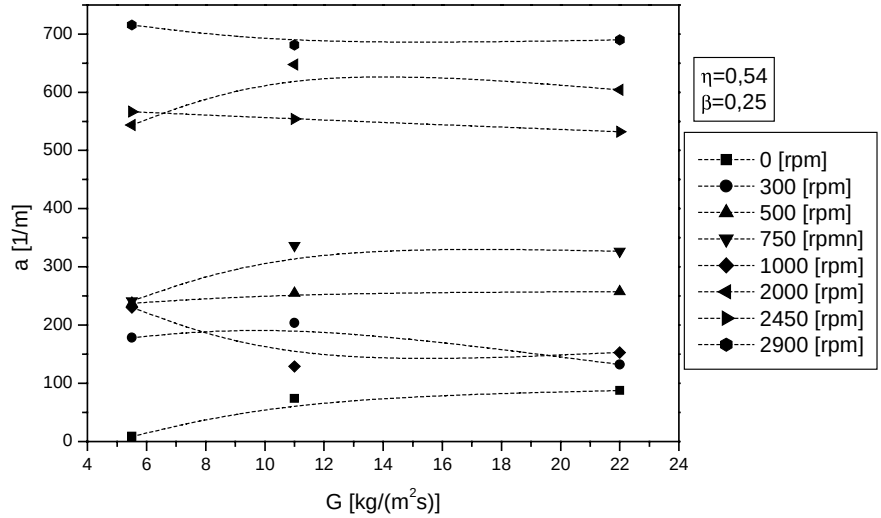

Fig. 13. Dependence of interfacial area on the rotational speed of impeller on the liquid axial flow rate for $\eta = 0.54$ and $\beta = 0.25$.

cial area on the rotational speed of impeller obtained by the method of chemical absorption of carbon dioxide in aqueous solutions of diethanoloamine confirm the earlier conclusions. Very good coincidence of the results obtained from both methods within the low values of the rotational speed of rotor is evident. At higher values of this parameter a significant discrepancy appears between the data. Because of large values of $k_L a$ in helicoidal reactor (as it was mentioned in Section 1, of the order of $10^{-1}\,s^{-1}$ [13,14]), increasing with increased rotor rotational speed, in order to avoid a possibility of carbon dioxide exhaustion due to its absorption, it was necessary to apply in the experiments higher values of the initial concentration of CO_2 in the gas phase. The method of interfacial area determination using DEA solutions is based on application of very diluted gaseous solutions [30]. Such a condition could not be fulfilled in the case of higher rotation speed of rotor accompanied by high absorption rates of CO_2. It is then concluded that the method based on using CO_2 absorption in DEA solutions under conditions where absorption proceeds at a limited rate is not suitable for use in helicoidal reactors.

Comparison of changes in the values of interfacial area and the volumetric mass transfer coefficient with hydrodynamic flow parameters indicates that interfacial area depends mainly on the rotational speed of rotor (Figs. 2 and 3), and, to a much less extent, on the axial flow velocity (Fig. 13). The values of the mass transfer coefficient both depend on the rotational speed of rotor as well as on the axial flow velocity as it results from superposition of two types of flow. As an example Figs. 14 and 15 show dependencies of the values of the volumetric mass transfer coefficient and the estimated mass transfer coefficients on the linear velocity expressed by the liquid mass flux at constant rotational speeds of rotor. The estimated values of k_L are of the order of 10^{-5}

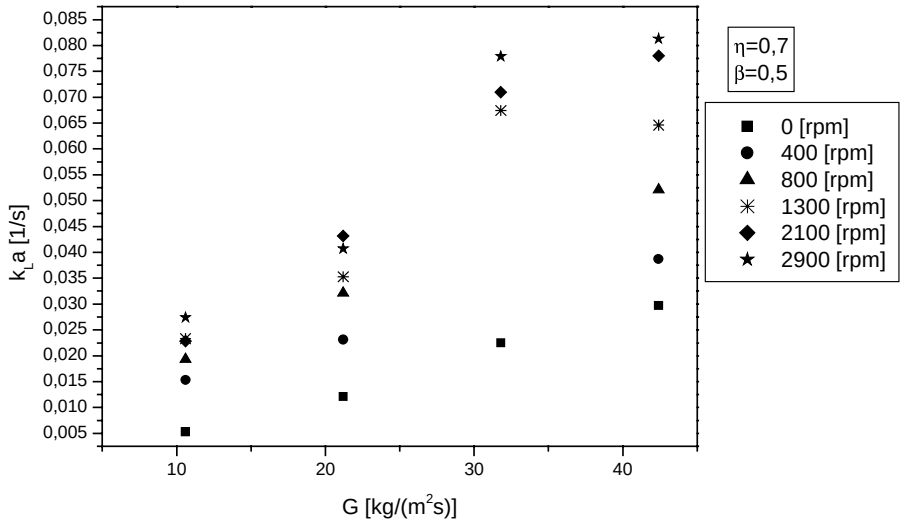

Fig. 14. Dependence of the volumetric mass transfer coefficient on the liquid axial flow rate for $\eta = 0.7$ and $\beta = 0.5$.

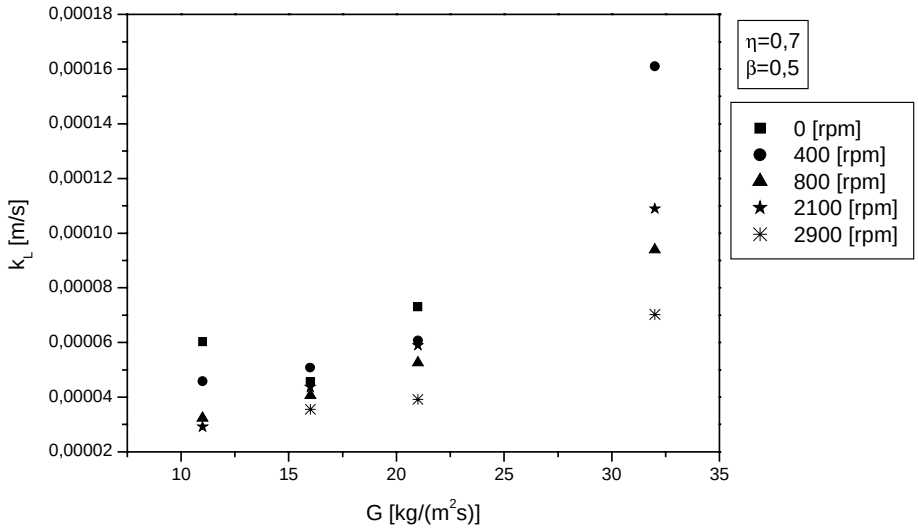

Fig. 15. Dependence of the mass transfer coefficient on the liquid axial flow rate for $\eta = 0.7$ and $\beta = 0.5$.

to 10^{-4} m/s, corresponding to those obtained in other reactors operating with dispersed gas–liquid systems.

5. Summary

1. The investigations revealed that interfacial area in the system gas–liquid in helicoidal reactor is high (of the order of 10^3 m^{-1}) and to a great extent it depends on the flow regime, i.e. on the rotation speed of rotor and to some extent on the gap width (in particular for narrow gaps). Small effect of the liquid axial flow was found. The values of the interfacial area obtainable in helicoidal reactor are typically greater than those encountered in tank reactors equipped with impellers ([31]).
2. A correlation between changes in the interfacial area and changes in the flow structure within the reactor was also observed. This makes it possible to suggest a hydrodynamic model of the reactor for three fundamental regions (Figs. 6 and 7):

- cocurrent gas–liquid slug flow (regions 1 on the map);
- two-phase flow with vortices (concept of continuos stirred tank reactors in series) (regions 2);
- ring flow of parallel vortices of liquid (i.e. mostly liquid) and gas (i.e. mostly gas) phases (region 3) [32].

These are the relevant conclusions when the reactor may be implemented to carry out complex reactions (selective, consecutive, etc.).

Notation

a	interfacial area related to a unit volume of reactor [m^{-1}]
d_m	mean bubble diameter [m]
D_{O_2}	oxygen diffusivity in the liquid phase [m^2/s]
D_i	rotor diameter [m]
D_o	outer cylinder diameter [m]
G	mass flux [kg/(m^2 s)]
k	reaction rate constant [m$^{1.5}$/(mol$^{0.5}$ s)]
k_L	mass transfer coefficient [m/s]
L	length of reactor [m]
N	rotational speed of impeller [rpm]
$[O_2]_i$	oxygen molar concentration at the interface [kmol/m^3]
P	dissipated power resulting from the rotational motion of rotor estimated as for a single-phase flow referred to a unit volume of reactor [W/m^3]
$[S_2O_4^{2-}]$	sodium dithionite concentration [kmol/m^3]
u_L	liquid superficial velocity [m/s]
β	volumetric flow ratio of gas and liquid at the reactor inlet
$\eta = D_i/D_o$	ratio of the rotor and outer cylinder diameters

Acknowledgements

This study has been carried out within the financial support of the Committee of Scientific Investigations (KBN, Poland) in the frame of a Scientific Grant No. K013/T09/01i/2000.

References

[1] G.I. Taylor, Stability of a viscous liquid contained between two rotating cylinders, Philos. Trans. R. Soc. London, Ser. A 223 (1923) 243–289.
[2] A.H. Snyder, Experiments on the stability of spiral at low axial Reynolds numbers, Proc. R. Soc. A 265 (1962) 198–214.
[3] R.M. Lueptow, A. Docter, K. Min, Stability of axial flow with a rotating inner cylinder, Phys. Fluids A 4 (11) (1992) 2446–2455.

[4] G. Desmet, H. Verelst, G. Baron, Local and global dispersion effects in Couette–Taylor flow—I. Description and modeling of the dispersion effects, Chem. Eng. Sci. 51 (1996) 1287–1298.
[5] G. Desmet, H. Verelst, G. Baron, Mixing characteristics of a Couette–Taylor bioreactor with gel-entrapped cells, in: Proceedings of the Seventh European Congress on Mixing, Koninklijke Vlaamse Ingenieurs Vereninging, Antwerp, 1991.
[6] M.M. Resende, P.W. Tardioli, V.M. Fernandez, A.L.O. Ferreira, R.L.C. Giordano, Distribution of suspended particles in a Taylor–Poiseuille vortex flow reactor, Chem. Eng. Sci. 56 (2001) 755–761.
[7] J.G. Sczechowski, C.A. Koval, R.D. Nobel, A Taylor vortex reactor for heterogeneous photocatalysis, Chem. Eng. Sci. 50 (1995) 3163–3173.
[8] K. Kataoka, N. Ohmura, M. Kouzu, Y. Simamura, M. Okubo, Emulsion polimerization of styrene in a continuous Taylor vortex flow reactor, Chem. Eng. Sci. 50 (9) (1995) 1409–1416.
[9] S. Lee, R.M. Lueptow, Rotating reverse osmosis: a dynamic model for flux and rejection, J. Membr. Sci. 192 (2001) 129–143.
[10] W.M. Jung, S.H. Kang, W.S. Kim, C.K. Choi, Particle morphology of calcium carbonate precipitated by gas–liquid reaction in a Couette–Taylor reactor, Chem. Eng. Sci. 55 (2000) 733–747.
[11] G.A. Ameer, E.A. Grovender, B. Obradovic, C.L. Cooney, R. Langer, RTD analysis of novel Taylor–Couette flow device for blood detoxification, AIChE J. 45 (3) (1999) 633–638.
[12] S. Wroński, E. Dłuska, R. Hubacz, E. Molga, Mass transfer in gas–liquid Couette–Taylor flow in membrane reactor, Chem. Eng. Sci. 54 (1999) 2963–2967.
[13] E. Dłuska, S. Wroński, R. Hubacz, Mass transfer in gas–liquid Couette–Taylor flow reactor, Chem. Eng. Sci 56 (2001) 1131–1136.
[14] E. Dłuska, S. Wroński, T. Ryszczuk, Mass transfer and interfacial area in gas–liquid Couette–Taylor flow reactor, in: Proceedings of the Sixth World Congress of Chemical Engineering, Melbourne, 23–27 September, 2001.
[15] R. Hubacz, Hydrodynamic of two-phase flow in helicoidal reactor, Ph.D. thesis, Warsaw University of Technology, 2003 (in Polish).
[16] R. Hubacz, S. Wroński, Horizontal Couette–Taylor flow in two-phase gas–liquid system flow patterns, Exp. Therm. Fluid Sci. 28 (2004) 457–466.
[17] Committee on Analytical Methods, Am. Dyestuff Reptr. 46 (1957) 443.
[18] A.S. Jhaveri, M.M. Sharma, Absorption of oxygen in aqueous alkaline solutions of sodium dithionite, Chem. Eng. Sci. 23 (1968) 1–8.
[19] A.S. Jhaveri, M.M. Sharma, Effective interfacial area in a packed column, Chem. Eng. Sci. 23 (1977) 669–676.
[20] B.N. Sahay, M.M. Sharma, Absorption in packed bubble columns, Chem. Eng. Sci. 28 (1973) 2245–2255.
[21] J.B. Joshi, M.M. Sharma, Mass transfer and hydrodynamic characteristics of gas inducing type of agitated contactors, Can. J. Chem. Eng. 55 (1977) 683–695.
[22] F. Camacho, M.P. Paez, G. Blazquez, J.M. Garrido, Oxygen absorption in alkaline sodium dithionite solutions, Chem. Eng. Sci. 47 (1992) 4309–4314.
[23] F. Camacho, M.P. Paez, G. Blazquez, M.C. Jiminez, M. Fernandez, Influence of pH on the oxygen absorption kinetics in alkaline sodium dithionite solutions, Chem. Eng. Sci. 50 (1995) 1181–1186.
[24] F. Camacho, M.P. Paez, M.C. Jiminez, M. Fernandez, Application of the sodium dithionite oxidation to measure oxygen transfer parameters, Chem. Eng. Sci. 52 (1997) 1387–1391.
[25] P.V. Danckwerts, Gas–Liquid Reactions, McGraw Hill, New York, 1970.
[26] J.C. Charpentier, Mass transfer rates in gas–liquids absorbers and reactors, in: T.B. Drew, G.R. Cokelet, J.W. Hoopes Jr., T. Vermeulen (Eds.), Advances in Chemical Engineering, vol. 11, Academic Press, New York, 1981, pp. 1–133.
[27] W. Moniuk, R. Pohorecki, A. Zdrójkowski, Measurements of mass transfer coefficients in liquid phase in stirred reactor, Rep. Faculty Chem. Process Eng. Warsaw Univ. Technol. 24 (3–4) (1997) 177–197 (in Polish).
[28] T. Ryszczuk, S. Wroński, Measurements of interfacial area in helicoidal reactor, Rep. Faculty Chem. Process Eng. Warsaw Univ. Technol. 29 (2004) 15–23.
[29] T. Ryszczuk, Measurements of interfacial area in helicoidal reactor, Ph.D. thesis, Warsaw University of Technology, 2003 (in Polish).
[30] E.J. Molga, K.R. Westerterp, Gas–liquid interfacial area and holdup in a cocurrent upflow packed bed bubble column reactor at elevated pressures, Ind. Eng. Chem. Res. 36 (1997) 622–631.
[31] A. Gianetto, P.L. Silveston., Multiphase Chemical Reactors, Hemisphere Publishing Corporation, Washington, USA, 1986, p. 41, Table 2-1.
[32] S. Wroński, E. Dłuska, J. Woliński, Oxidation of the organic liquids in helical reactor modelling of the reactors performance, Pol. J. Chem. Technol., in preparation.